Aspects Regarding the Attitude Correction for Small Sized Satellites, using Electric Motors

Boboc C., Andrei I.
ICPE
Bucharest, Romania
cristianboboc.messico@icpe.ro,
iulianandrei.messico@icpe.ro

Modreanu M., Jula N.
Academia Tehnica Militara,
Bucharest, Romania
mirceamodreanu.messico@icpe.ro,
nicolae.jula@gmail.com

***Abstract* — The paper presents the electromagnetic modelling methodologies of a DC brushless motor for space application, by using specialized software for the numeric field analysis COMSOL Multiphysics. In the first part are presented the results of the modeling, in the second part, the numeric results of the model will be compared and validated by the experimental one.**

***Key words* — numeric modeling, DC Brushless motor.**

I. INTRODUCTION

The development of small sized satellites has shown an accelerated increase in the last years due to the opportunity to access the outer space with relatively low costs and the short time required for developing such a satellite (equipment). The satellites from this class, known as Cube-Sat, have proven useful both in the scientific field and for demonstrations for new technologies, up to date more than 120 satellites from this category have been launched [12].

The standard Cube-Sat assumes the development of a cube shaped satellite, with the edge length of 0.01 m, with a maximum mass of 1 kg [12].

To achieve the mission for such a satellite, an important role is played by the subsystem for attitude determination and control that represents the orientation of the satellite around its own mass center to an external reference system (Earth, Sun, local magnetic field, another satellite, etc.).

Generally, a permanent control of the altitude of a satellite is required both for the optimization of the solar energy collection and for positioning in the external reference system with a certain accuracy, when scientific experiments are conducted onboard the satellite.

One of the procedures that can be used for changing the attitude (position) of a Cube-Sat type satellite is based on the brushless direct current motor, with high speed and axial air gap.

The restrictions for dimensions and weight, for the mounting of this electric motor, imposed a flattened construction, presented in fig. 1, in which are also displayed the main components of the electric motor assembly.

Components of the motor from fig. 1:
1. Flat coil fitting, 2. ball bearing support, 3. ball bearing, 4. magnet, 5. rotor fitting, 6. axle.

The advantages that recommend the use of this type of motor for our purpose are:
- flattened construction.
- very good power/volume ratio.
- low current.
- very long life span.
- in the version with Hall sensors, the speed is very accurately controlled.

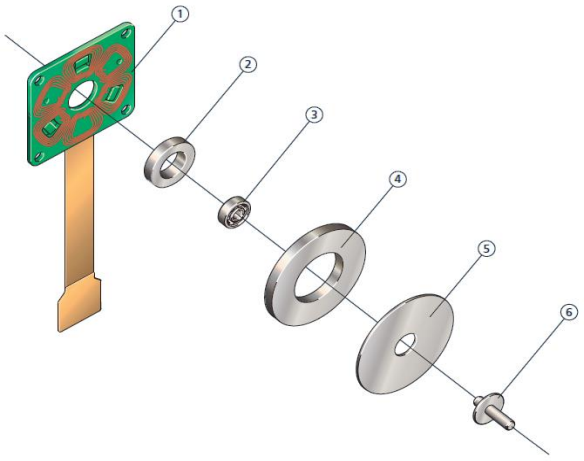

Fig. 1. Electric motor body.

For the attitude control are employed three electric motors mounted on three faces of the satellite.

The three electric motors actuate three flywheels, which generate the torque required for the rotation of the satellite on the axes Ox, Oy and Oz.

Such a system has the advantage of operating using the principle of conservation of kinetic momentum (if one of the flywheels is accelerated in one direction, the satellite will be accelerated in the opposite direction). In this case, the mass of the whole system remains constant, unlike the systems that use fuel powered motors, a resource that is decreased during the mission, altering the mass and the center of mass of the satellite.

Within this paper are presented the main aspects regarding the calculation method for the electric motor, the various models with their results and the experimental model of the

motor executed within a project with the European Space Agency.

II. Modeling And Simulations Employed For The Determination Of The Parameters Of The electric Motor

The numerical modeling was conducted in a program for the analysis of the electromagnetic field, Comsol Multiphysiscs, which is based on the finite element method. This method is used in order to obtain some specific characteristics of the motor, required for the designing, like: Value and shape of the magnetic induction in the motor air gap, the characteristic torque - angle for an impressed current, the curve of electromotor voltage, etc.

The modeling was conducted based on the dimensions from the electromagnetic theory characterized by general laws and materials laws, written in the local form. The laws applied for the study of the characteristics of the electric motor are:

- the law of the magnetic circuit

$$rot\boldsymbol{H} = \boldsymbol{J_e}; \quad (1)$$

In which H is the intensity of the magnetic field, and Je is the density of the induction current.

- the law of the magnetic flux

$$div\boldsymbol{B} = \boldsymbol{0}; \quad (2)$$

Where B represents the magnetic induction

Written in another form, by introducing the magnetic potential vector, applied for this case, the formula becomes.

$$\boldsymbol{B} = rot\boldsymbol{A} \quad (3)$$

Where A is the magnetic potential vector

- The law of the link between the magnetic induction, the intensity of the magnetic field and the magnetization

$$\boldsymbol{B}=\mu_0(\boldsymbol{H}+\boldsymbol{M}) \quad (4)$$

In which M is the magnetization of the body, and $\mu_0=4\pi 10^{-7}$ is the permissiveness of the vacuum in IS.

For the defining of the coils is used a feature of the program that allows the defining of a coil with multiple windings on a 3D domain, specifying the number of windings N, the area of the conductor a_{coil} and the injected current I_{coil}. The current exciting is defined by the current density give by:

$$J_e = \frac{N \cdot I_{coil}}{A}, \quad (5)$$

Where A is the total area of the section of the conductor domain.

The numerical analysis program employs Maxwell's tensor T_2, which in a magnetic field is given by the formula

$$n_1 T_2 = -\frac{1}{2} n_1 (H \cdot B) + (n_1 \cdot H) B^T, \quad (6)$$

The calculation of the torque with the aid of Maxwell's tensor is given by the formula:

$$M_O = \oint_{\partial \Omega} (r - r_O) \times (n_1 \cdot T_2) dS. \quad (7)$$

The finite element method (FEM) represents one of the most widespread instruments for solving differential equations in various fields, among which is the electromagnetism field.

The first step of the numerical modeling is the development of the geometrical model presented in fig. 2. The problem was modeled in 3D, because the motor has an axial air gap. In addition, the motor has a very small length compared to its diameter and the end effects can not be neglected. For the modeling, were included only the parts that are important from an electromagnetic perspective: The rotor (rotor fitting and permanent magnets) and stator (only the winding part).

The characteristics regarding the materials employed in the numerical model are:

- Steel for the rotor fitting (characteristic BH in Fig.3).
- The rare earth permanent magnets of the type NdFeB 37 (Br = 1,219T, coercive field H_c= 964 kA/m, $(BH)_{max}$=37 MGOe);
- Copper for the construction of the coils.
- For the rest of the calculation domain the environment was considered as being the air.

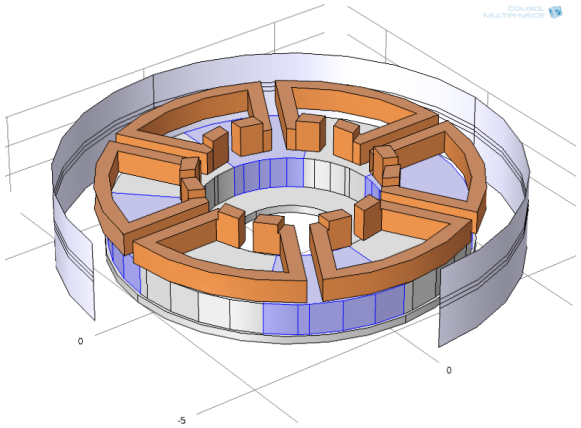

Fig. 2. Geometric model of the electric motor.

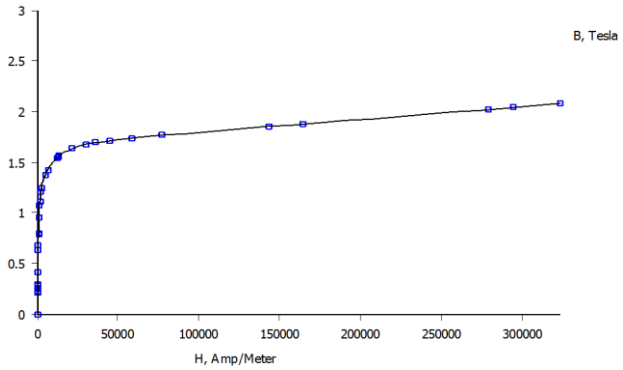

Fig. 3. BH characteristic for the rotor fitting.

The quantizing network presented in fig. 4 is composed from regular tetrahedrons and was selected in a non-uniform fashion so that it will be denser in the air gap of the motor. At various angles of the rotor to the stator the systems of

equations resulted had a number of different degrees of freedom, between $3.2*10^6$-$5.8*10^6$ degrees of freedom.

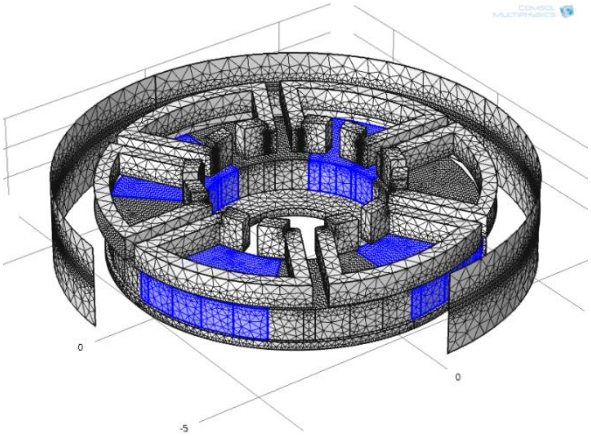

Fig. 4. Quantization network for the numerical model.

For the running of the numerical system was employed a high performance computing system, the ATLAS cluster, from the University "Politehnica" Bucharest. For the solving of the system resulted from the quantization was employed an iteration method with preconditioning, more precisely the improved generalized residual method (GRES and SOR). Using this solver, a system with $3.2*10^6$-$5.8*10^6$ degrees of freedom was solved in 22, respectively 46 minutes, with a RAM memory consumption between 23-37 GB.

In fig. 5 is presented the component on the Oz axis for the magnetic induction, from which can be observed the N-S alternation of the magnetic poles of the motor.

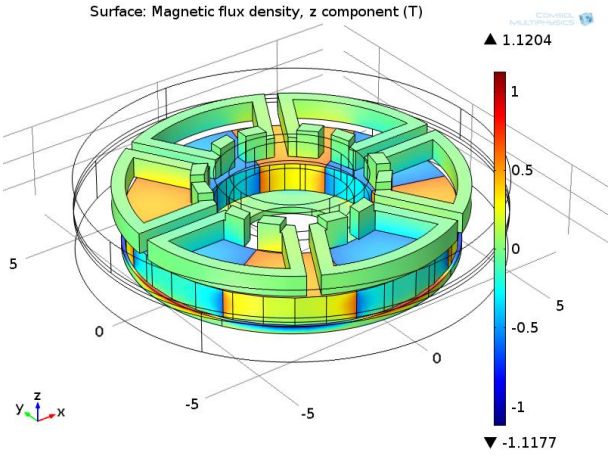

Fig. 5. Component of the magnetic induction on the axis Oz.

Fig. 6 represents the distribution of the magnetic field in the motor, the sources of electromagnetic field being the permanent magnets and the currents injected in the winding.

The most important area for the calculation of a motor is the air gap area.

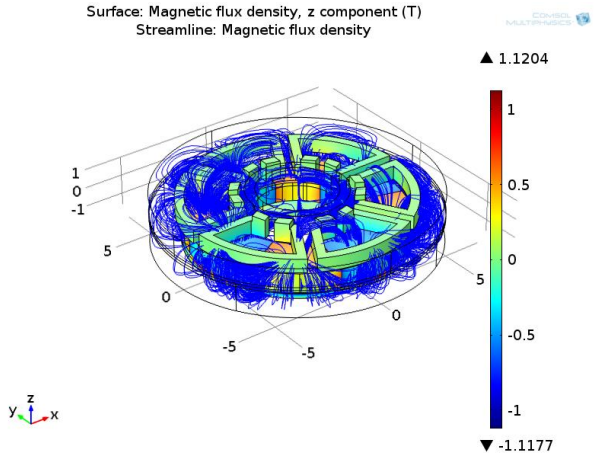

Fig. 6. Distribution of the magnetic field induction in the motor.

The accuracy of the numerical results is strongly influenced by the quantization degree for this area. In fig. 7 is presented the component on the axis Oz for the magnetic induction, in a section positioned at the middle of the distance between the rotor surface and the one of the stator winding. The numerical calculation was employed to determine the value of the motor torque for different relative positions rotor - stator, when the two phases are powered.

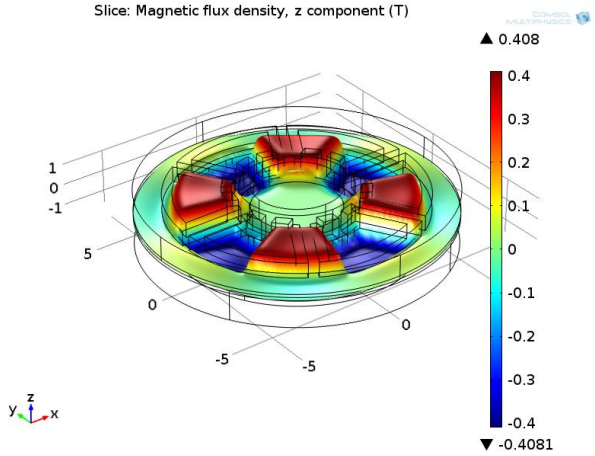

Fig. 7. Distribution of the magnetic induction in the air gap.

The characteristic torque - angle is presented in fig. 8 and represents the variation on a pair of poles (90 electrical degrees) of the electromagnetic torque. Can be observed the sinusoidal variation, which is pretty clear for the characteristic (no interference torques), with a maximum torque of 0.054 mNm.

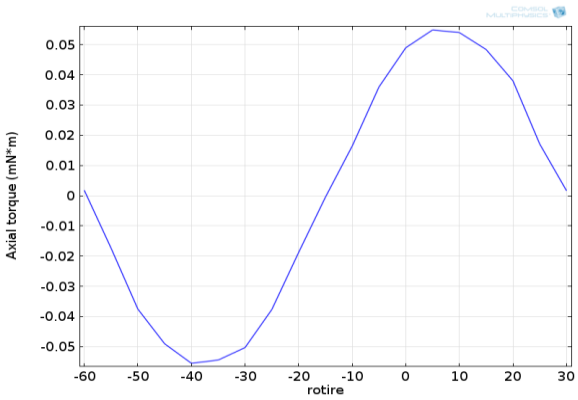

Fig. 8. Characteristic torque - angle.

III. Experimental Model Developed And Results Obtained

Based on the numerical modeling was developed an experimental model, more precisely a brushless direct current motor with axial air gap.

The designed and manufactured motor has 2p = 8 poles, as such, the magnetic ring is composed from 8 permanent magnet segments with identical shape and dimensions, fixed by gluing, so that the polarities of two adjacent magnets will alternate. The permanent magnets have high magnetic energies, type neodymium - iron - boron 37.

The magnets NdFeB 37 have the following technical characteristics: Remnant induction B_r = 1.219T, coercive field H_c= 964 kA/m, $(BH)_{max}$=37 MGOe, coefficient for induction variation by temperature –0.11%/°C, coefficient for magnetic field variation by temperature –0.55%/°C.

The assembly magnet - ferromagnetic fitting united with the motor axle forms the motor rotor. Even if it is constructively simple, this assembly must operate as a resistant structure, with good dynamic balancing, vibration free, in the revolutions interval 40 000 ÷ 60 000 rpm.

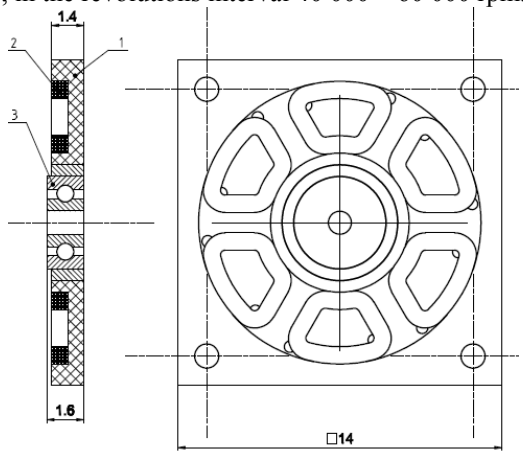

Fig. 9. Components of the stator subassembly presented:
1. Processed stator plate, 2. Coil, 3. Ball bearing.

For the stator was selected a triple phased winding diagram, which does not present overlapping of coil heads, thus facilitating the obtaining of a very thin flat winding. The winding of the stator is characterized by the following parameters: Triple phased winding m = 3, number of pole pairs p = 4, number of notches by pole and phase q = 1/4. The six coils that have the shape presented in fig. 10, are made with an insulated conductor, provided with a layer of thermal adhesive varnish that allows the consolidation of the coils by pre-forming.

The six coils are mounted on a stator plate processed from an electrically insulating material based on fiber glass, copper plated, like shown in fig. 10. As can be observed in fig. 10 and 11, on one side of the plate is processed a channel like a circular crown, with holes for the terminals of the six coils. On the other side of the plate is a circuit board that ensures the connections between the phase coils.

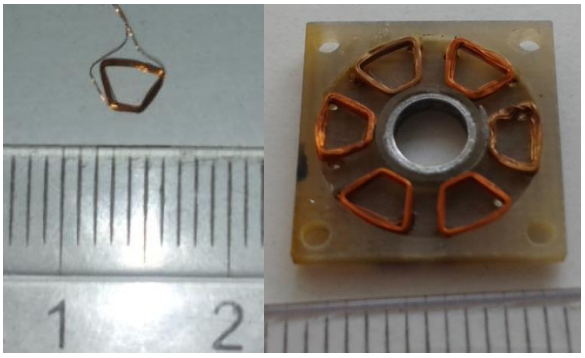

Fig. 10. Coil and mounted winding assembly.

Figure 11 represents pictures with the manufactured experimental model, the first part representing the motor by subassemblies, and the second part representing the mounted motor. The experimental model observes the already presented documentation and manufacturing technology.

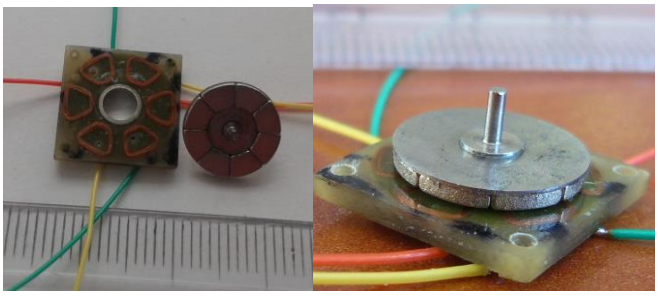

Fig. 11. General view of the composing subassemblies and mounted experimental model assembly.

Considering the reversibility of the electrical machines, in order to determine the characteristics of the motor, it was tested as a generator, its rotor being actuated at 1000 rpm. The oscillograms from figures 12 and 13 represent the voltage for phase A, respectively the electromotor voltages (TE) for the three phases, collected simultaneously.

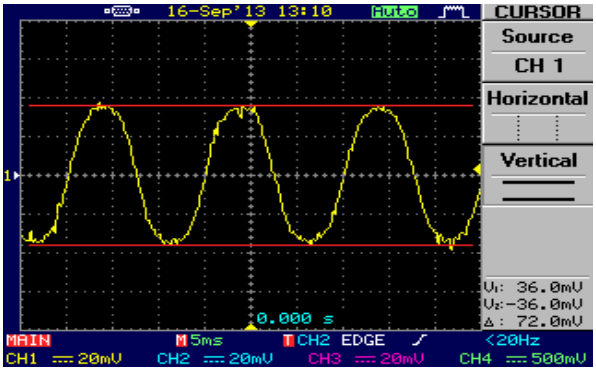

Fig. 12. Oscillogram for TE on phase A.

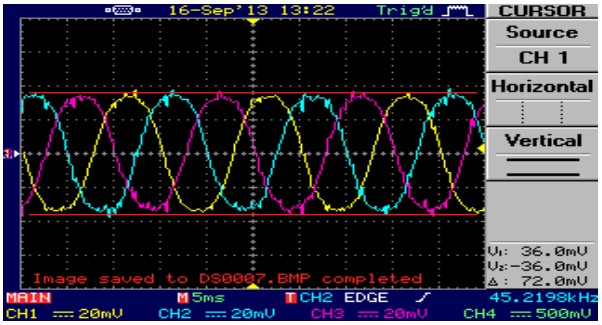

Fig. 13. Oscillogram for TE on the 3 phases ABC.

Figures 14 and 15 present the line electromotor voltages (two series phases), the first with the values shown by the device, and the second with the values measured between the limits fixed by the operator. Can be observed the sinusoidal shape of the characteristic, with a peak value of 68 mV.

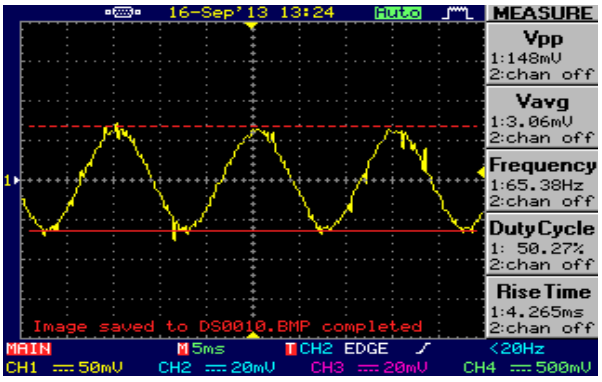

Fig. 14. Line TE, displayed value.

CONCLUSIONS

As we specified, from the presented numerical model, is obtained the toque constant for the motor k_M=0.647mNm/A. It corresponds to the constant of the electromotor voltage k_E=0.0677mV/rpm.

As a result of the measurements conducted on the experimental model was obtained the constant of the electromotor voltage k_E=0.0628mV/rpm.

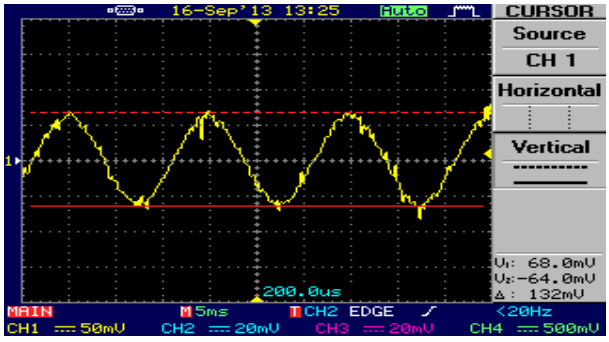

Fig. 15. Line TE, imposed limits.

Can be observed a difference between the numerical and the experimental model of 7.8%, which is completely acceptable considering the accuracy of the construction of an experimental model, and also the precision of the numerical calculation method. The differences can be explained by certain aberrations that exist in the experimental model (shape and dimensions of the coils, positioning of the coil from the magnets - distance and non-parallelism).

REFERENCES

[1] D. Stoia, "Motoare de curent continuu excitate cu magneţi permanenţi", Editura Tehnica, Bucureşti 1983.

[2] Moog Catalogue, "Direct Drive Brushless DC Torque Motors", 2013.

[3] R. Măgureanu, "Maşini electrice speciale pentru sisteme automate", Editura Tehnică, Bucharest, 1981.

[4] T. Tudorache, M. Morega, "Calculul 3D al încălzirii unui motor de c.c. de mică putere folosind metoda elementului finit", Simpozionul Actualităţi şi Perspective în domeniul maşinilor electrice, Ediţia a V-a, Universitatea POLITEHNICA din Bucureşti, Catedra de Maşini, Acţionări şi Materiale, 13 – 14 octombrie 2009, ISSN 1843-5912.

[5] O. Craiu, A. Machedon, "3D finite element thermal analysis of a small power pm dc motor – optim", 12th International Conference on Optimization of Electrical and Electronic Equipment, Brasov, 20-22 mai 2010.

[6] O. Craiu, A. Machedon, "Modele electromagnetice si termice pentru servomotoare de c.c. cu magneti permanenti", Tendinţe de dezvoltare în fabricaţia maşinilor electrice şi cerinţe actuale ale UE, Universitatea POLITEHNICA din Bucureşti, 15 Apr. 2010.

[7] COMSOL Multiphysics Documentation http://www.comsol.com/.

[8] J.-M. Jin, "The Finite Element Method in Electromagnetics", John Wiley and Sons Publisher, New York, 2002.

[9] A. Bondeson, T. Rylander, and P. Ingelstrom,

[10] "Computational Electromagnetics", Springer, 2005.

[11] D. Meeker, "User's Manual for Finite Element

[12] Method Magnetics – FEMM", ver. 4.2, Oct. 2010.

[13] Y. Saad, "Iterative Methods for Sparse Linear Systems", Second Edition, Society for Industrial and Applied Mathematics – SIAM Publisher, 2003.

[14] [*] http//:en.wikipedia.org/wiki/list-of-cubesat

[15] [*] http//:www.cubesat.org